Two-dimensional grating for narrow-band filtering with large angular tolerances

Evgeny Popov,[1,*] Anne-Laure Fehrembach,[1] Yoann Brûlé,[1] Guillaume Demésy,[1] and Philippe Boyer[2]

[1]*Aix Marseille Université, CNRS, Centrale Marseille, Institut Fresnel UMR 7249, Fac. St. Jérôme, 13397, Marseille, France*

[2]*Département d'Optique P.-M. Duffieux, Institut FEMTO-ST, CNRS UMR 6174, Université de Franche-Comté, 25030 Besançon Cedex, France*

[*]*e.popov@fresnel.fr*

Abstract: A two-dimensional periodic sub-wavelength array of vertical dielectric cylinders on a glass substrate is studied numerically using three different electromagnetic approaches. It is shown that such structure can present a narrow-band spectral resonance characterized by large angular tolerances and 100% maximum in reflection. In particular, in a two-nanometer spectral bandwidth the reflectivity stays above 90% within angles of incidence exceeding 10 degrees for unpolarized light. Bloch modal analysis shows that these properties are due to the excitation of a hybrid mode that is created in the structure by a guided-like mode and a localized cavity mode. The first one is due to the collective effect of the array, while the second one comes from the mode(s) of a single step-index fiber.

OCIS codes: (050.0050) Diffraction and gratings; (050.2770) Gratings; (050.6624) Subwavelength structures.

References and links

1. D. Rosenblatt, A. Sharon, and A. A. Friesem, "Resonant grating waveguide structures," IEEE J. Quantum Electron. **33**(11), 2038–2059 (1997).
2. A. Sentenac and A.-L. Fehrembach, "Angular tolerant resonant grating filters under oblique incidence," J. Opt. Soc. Am. A **22**(3), 475–480 (2005).
3. F. Lemarchand, A. Sentenac, and H. Giovannini, "Increasing the angular tolerance of resonant grating filters with doubly periodic structures," Opt. Lett. **23**(15), 1149–1151 (1998).
4. A.-L. Fehrembach, F. Lemarchand, A. Talneau, and A. Sentenac, "High Q polarization independent guided-mode resonance filter with "doubly periodic" etched Ta2O5 bidimensional grating," IEEE J. Light. Tech. **28**, 2037–2044 (2010).
5. X. Buet, E. Daran, D. Belharet, F. Lozes-Dupuy, A. Monmayrant, and O. Gauthier-Lafaye, "High angular tolerance and reflectivity with narrow bandwidth cavity-resonator-integrated guided-mode resonance filter," Opt. Express **20**(8), 9322–9327 (2012).
6. K. Kintaka, T. Majima, J. Inoue, K. Hatanaka, J. Nishii, and S. Ura, "Cavity-resonator-integrated guided-mode resonance filter for aperture miniaturization," Opt. Express **20**(2), 1444–1449 (2012).
7. O. Parriaux, T. Kämpfe, F. Garet, and J.-L. Coutaz, "Narrow band, large angular width resonant reflection from a periodic high index grid at terahertz frequency," Opt. Express **20**(27), 28070–28081 (2012).
8. A. Taghizadeh, J. Mørk, and I.-S. Chung, "Ultracompact resonator with high quality-factor based on a hybrid grating structure," Opt. Express **23**(11), 14913–14921 (2015).
9. Y. Wang, D. Stellinga, A. B. Klemm, C. P. Reardon, and T. F. Krauss, "Tunable optical tilters based on Silicon Nitride high contrast gratings," IEEE J. Sel. Top. Quantum Electron. **21**, 2700706 (2015).
10. R. Magnusson and M. Shokooh-Saremi, "Physical basis for wideband resonant reflectors," Opt. Express **16**(5), 3456–3462 (2008).
11. C. F. R. Mateus, M. C. Y. Huang, Y. Deng, A. R. Neureuther, and C. J. Chang-Hasnain, "Ultrabroadband mirror using low-index cladded subwavelength grating," IEEE. Phot. Tech. Lett. **16**(2), 518–520 (2004).
12. L. Chen, M. C. Y. Huang, C. F. R. Mateus, C. J. Chang-Hasnain, and Y. Suzuki, "Fabrication and design of an integrable subwavelength ultrabroadband dielectric mirror," Appl. Phys. Lett. **88**(3), 031102 (2006).
13. P. Lalanne, J.-P. Hugonin, and P. Chavel, "Optical properties of deep lamellar gratings: a Coupled Bloch-mode insight," J. Light. Tech. **24**(6), 2442–2449 (2006).
14. V. Karagodsky, F. G. Sedgwick, and C. J. Chang-Hasnain, "Theoretical analysis of subwavelength high contrast grating reflectors," Opt. Express **18**(16), 16973–16988 (2010).

#264075 Received 26 Apr 2016; revised 14 Jun 2016; accepted 14 Jun 2016; published 23 Jun 2016

15. P. Qiao, L. Zhu, W. C. Chew, and C. J. Chang-Hasnain, "Theory and design of two-dimensional high-contrast-grating phased arrays," Opt. Express **23**(19), 24508–24524 (2015).
16. M. Shokooh-Saremi and R. Magnusson, "Properties of two-dimensional resonant reflectors with zero-contrast gratings," Opt. Lett. **39**(24), 6958–6961 (2014).
17. D. A. Bekele, G. C. M. R. C. I.-S. Park, R. Malureanu, and I.-S. Chung, "Polarization-independent wideband high-index-contrast grating mirror," IEEE Photonics Technol. Lett. **27**(16), 1733–1736 (2015).
18. L. Li, "New formulation of the Fourier modal method for crossed surface-relief gratings," J. Opt. Soc. Am. A **14**(10), 2758–2767 (1997).
19. L. Li, "Note on the S-matrix propagation algorithm," J. Opt. Soc. Am. A **20**(4), 655–660 (2003).
20. E. Popov and M. Nevière, "Maxwell equations in Fourier space: fast-converging formulation for diffraction by arbitrary shaped, periodic, anisotropic media," J. Opt. Soc. Am. A **18**(11), 2886–2894 (2001).
21. E. Popov, L. Mashev, and D. Maystre, "Theoretical Study of the Anomalies of Coated Dielectric Gratings," Opt. Acta (Lond.) **33**(5), 607–619 (1986).
22. A.-L. Fehrembach, D. Maystre, and A. Sentenac, "Phenomenological theory of filtering by resonant dielectric gratings," J. Opt. Soc. Am. A **19**(6), 1136–1144 (2002).
23. Ph. Boyer, G. Renversez, E. Popov, and M. Nevère, "Improved differential method for microstructured optical fibers," J. Opt. A, Pure Appl. Opt. **9**(7), 728–740 (2007).
24. G. Renversez, P. Boyer, and A. Sagrini, "Antiresonant reflecting optical waveguide microstructured fibers revisited: a new analysis based on leaky mode coupling," Opt. Express **14**(12), 5682–5687 (2006).
25. A. W. Snyder and J. D. Love, *Optical Waveguide Theory* (Kluwer Academic, Boston, 1983).
26. E. Popov, "Differential method for periodic media," ch.7 in *Gratings: Theory and Numeric Applications, Second Revisited Edition* (Institut Fresnel, PUP, Marseille, 2014).
27. G. Demésy, F. Zolla, A. Nicolet, and M. Commandré, "All-purpose finite element formulation for arbitrarily shaped crossed-gratings embedded in a multilayered stack," J. Opt. Soc. Am. A **27**(4), 878–889 (2010).
28. A. Nicolet, S. Guenneau, C. Guezaine, and F. Zolla, "Modelling of electromagnetic waves in periodic media with finite elements," J. Comput. Appl. Math. **168**(1-2), 321–329 (2004).

1. Introduction

Realizing a spectral filtering function with nanopatterned structures is not new but it is a still dynamic field of research. One advantage of nanopatterned structures over the interferential thin films filters is their smaller thickness, which is particularly interesting for applications in the far-infrared, where the thickness of the stacks needed is often an obstacle. Another advantage is that nanopatterned filters with different spectral characteristics can be created on a single chip, their filtering function can be differentiated by varying only few parameters of the pattern (for example the period, for a periodic pattern), preserving the same thickness of the assembly of different filters. On the contrary, fabricating an interferential thin films component with different filtering functions at adjacent points requires to modify the thickness of the films during their deposition. In other words, nanopatterned filters are more suitable to create pixelized filters, for example for spectroscopic imaging applications.

Furthermore, reducing the size of the pattern may be required, either to fulfill applications requirement (for pixelized filters for instance) or for fabrication reasons: a smaller pattern is etched within a shorter time, and will present less fabrication imperfections. Yet reducing the patterned size is possible only if the spectral function of the component is maintained when it is illuminated with a focused beam, which is particularly difficult to achieve together with a strong spectral selectivity. Narrow-band spectral filters can be achieved with the so-called Guided mode resonance filters (GMRF) composed of a subwavelength grating and a planar waveguide. The excitation of one eigenmode of the structure through one diffraction order of the grating generates a very narrow spectral peak in reflection (or transmission) [1], but with a very weak angular acceptance [2]. The excitation of two counter propagating modes generates a localized mode, which still presents a strong spectral selectivity but having a better angular acceptance. The angular acceptance can be further enhanced by increasing the interaction between the two counter propagating modes, either thanks to a complex basic periodic pattern [3,4], or by putting the GMRF in a box made of surrounding Bragg mirrors [5,6].

Another way to achieve a strong angular tolerance together with a strong spectral selectivity is to create a strongly localized resonance either by using a very high index material or high etching thicknesses [7–9]. In these, so called "High contrast grating", the coupling between a mode similar to the guided mode of a planar waveguide and a cavity mode leads to a hybrid mode [10], which presents a high angular tolerance, and having either a high spectral selectivity in the reflectivity [7–9] or a high reflectivity over a wide spectral

#264075 Received 26 Apr 2016; revised 14 Jun 2016; accepted 14 Jun 2016; published 23 Jun 2016

range suitable to create broadband mirrors [11,12]. This phenomenon can be interpreted in terms of modes propagating along the ridges for two-dimensional (2D) structures [13,14] (invariant along one direction). Recently, it has been shown that the same phenomenon occurs in 3D structures composed of circular or square pillars periodically arranged along two directions [15,16], allowing to exhibit a polarization independent wideband mirror behavior [17].

In this paper, we report the numerical simulation of an angularly tolerant and polarization independent narrow band spectral filter created with a deep 2D grating made of circular cylinders. Contrary to the studies presented in [15–17], our aim is to create a narrow-band filter working in reflection. The design proposed here has a 2 nm wide reflection maximum maintained above 95% within an angular interval of several degrees around normal incidence in unpolarized light. We show that the wide angular acceptance is due to the formation of a hybrid mode composed of a guided mode and a cavity mode. In the first part of the paper, we present the reflectivity behavior of the deep circular rods grating. In the second part, we interpret its property using a modal analysis.

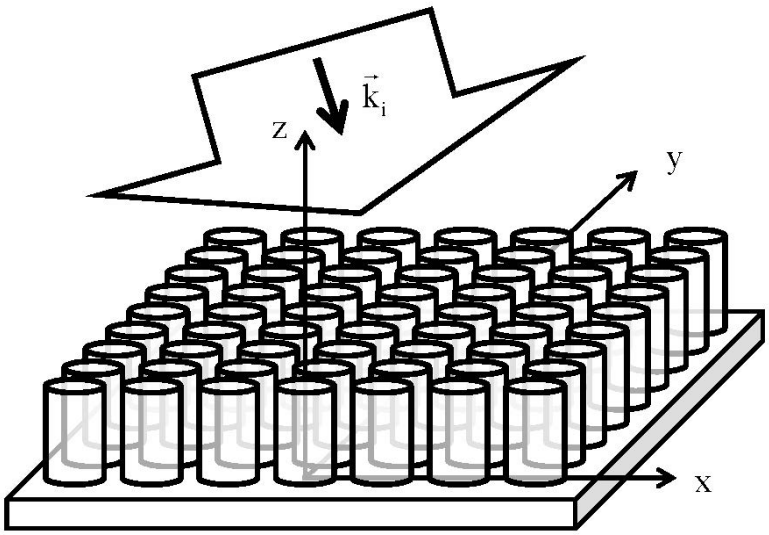

Fig. 1. Schematical presentation of a two-dimensional array of dielectric cylinders.

The structure under study presents a two-dimensional array of vertical dielectric cylinders oriented along the z axis represented schematically in Fig. 1. Their cross-section can have an arbitrary form, but we shall concentrate our attention to mainly circular cylinders. The periods in x- and y-direction are equal to d, and the wavelength λ is chosen so that near normal incidence there are no other than the 0th propagating orders in the cladding and the substrate.

The polar angle of incidence θ lies between the incident wavevector and the z-axis; the azimuthal angle of incidence φ lies between the plane of incidence ($\vec{k}_i$, Oz) and the x-axis. The incident polarization is linear and is defined with respect to the plane of incidence: as usual, it is called transverse electric (TE), when the electric field vector is perpendicular to the plane of incidence, and transverse magnetic (TM), when the electric field vector lies inside the plane of incidence.

2. Reflectivity behavior

In what follows, we consider a glass substrate (refractive index $n_s = 1.5$), a 2D periodical grating composed of cylinders with refractive index $n_f = 1.97$ embedded in air, the cladding is air. If $d = 0.5$ μm then, close to wavelength $\lambda = 0.865$ μm and normal incidence, there are only the 0th reflected and transmitted propagating orders. The map of the reflectivity in

#264075 Received 26 Apr 2016; revised 14 Jun 2016; accepted 14 Jun 2016; published 23 Jun 2016

normal incidence is presented in Fig. 2 as a function of the cylinder diameter Φ and its height h. Figure 2(a) covers a large interval of diameters and the practically interesting range of depths from 0 to 2 µm. The calculations were performed using a home-made numerical code based on the Fourier Modal Method [18] including the S-matrix propagation algorithm [19] and the Normal Vector Method [20] to perform a correct factorization of the product of discontinuous functions. Two different regions can be distinguished: (1) smaller diameters (up to 0.4 µm) with low reflectivity characterized by Fabry-Perot-like variations with h, that are more rapid for larger diameters; (2) a second region for longer and thicker cylinders, where fine and high maxima of the reflectivity can be observed, a zoom is presented in Fig. 2(b).

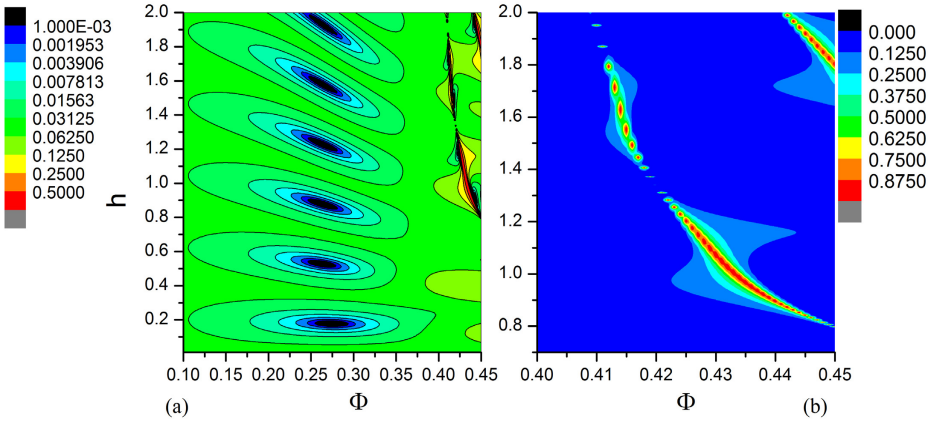

Fig. 2. Reflectivity of the dielectric grating in normal incidence as a function of the cylinder diameter and height given in microns. Period d = 0.5 µm, λ = 0.865 µm. (a) logarithmic scale over a large interval of diameters; (b) zoom of the upper right corner.

Two types of resonances are clearly visible with different speed of variation with Φ and h. Highest values of the reflectivity are obtained when two modes are simultaneously excited, as it is shown further on.

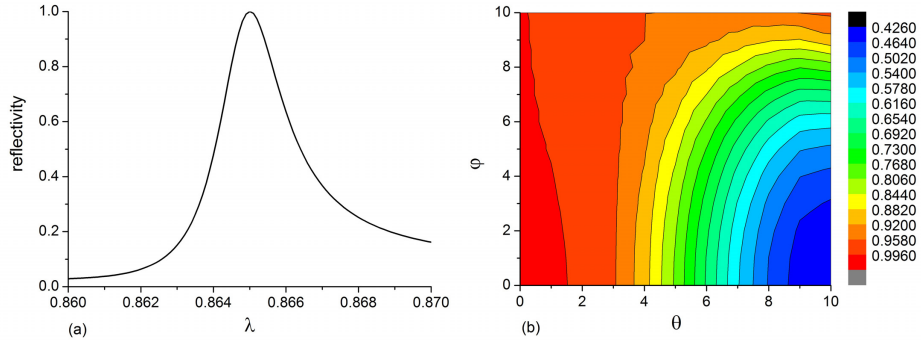

Fig. 3. (a). Spectral dependence of the reflectivity in normal incidence for d = 0.5 µm, h = 1 µm, Φ = 0.4333 µm; (b) Angular dependence of the reflectivity for λ = 0.865 µm, incident polarization along the x-axis. The other parameters as in Fig. 3.

Most interesting feature of the regions with high reflectivity is that it can reach 100% in a relatively small spectral interval, width at half-maximum around 2 nm in Fig. 3. Moreover, this specific resonance has very large angular tolerances (Fig. 4), suitable for smaller grating sizes and not well-collimated beams, as explained in the Introduction. The 100% value of the reflection maximum is due to the symmetry of the system. In particular, a geometry that has a vertical plane of symmetry is characterized by a presence of a real zero of the transmissivity

#264075 Received 26 Apr 2016; revised 14 Jun 2016; accepted 14 Jun 2016; published 23 Jun 2016

at resonance, due to the excitation of mode(s) of the system, thus the reflectivity can reach 100% at a resonance, as happens if Fig. 3. The mathematical explanation of this property in the case of 1D periodicity can be found in [21], and is extended to 2D periodicity in [22].

Next section is devoted to the modal analysis of these specific cases.

3. Modal analysis

In order to obtain a better physical understanding of the different types of behavior and of their cause, numerical tools enable us to "look" inside the diffraction process, for example, by subjecting it to a modal analysis of the grating structure (assuming that the rods are infinitely long), and how the incident plane wave couples to these modes.

For convenience, let us repeat the definition of the modes as given in the formulation of the Fourier modal method, an extension of the rigorous coupled-wave (RCW) theory to the two-dimensional periodicity. In a few words, the x and y components and the electric and magnetic fields are presented inside the grating region as a Fourier series in x and y (stored in a column vector F), whereas in z-direction the propagation constants γ are searched numerically as the eigenvalues of a given M-matrix, which contains the coefficients of the differential set of equation for F, derived from Maxwell equations:

$$\frac{d}{dz}F = M\,F. \tag{1}$$

The reconstruction of the field in the direct space is made using the matrix V containing the eigenvectors of M:

$$\begin{pmatrix} E_x \\ E_y \\ H_x \\ H_y \end{pmatrix} = \sum_{m,n,p} e^{ik_0(\alpha m x + \beta_n y)} V_{mn,p} e^{i\gamma_p z} b_p, \tag{2}$$

where b_p are the Bloch modal amplitudes, determined by applying the boundary conditions at $z = 0$ and h, and $k_0 = 2\pi / \lambda$. Equation (2) can be rewritten in an explicitly modal form:

$$\begin{pmatrix} E_x \\ E_y \\ H_x \\ H_y \end{pmatrix} = \sum_{p} \begin{pmatrix} E_{x,p}(x,y) \\ E_{y,p}(x,y) \\ H_{x,p}(x,y) \\ H_{y,p}(x,y) \end{pmatrix} e^{i\gamma_p z} b_p, \tag{3}$$

where the p-th modal field is given by

$$\begin{pmatrix} E_{x,p}(x,y) \\ E_{y,p}(x,y) \\ H_{x,p}(x,y) \\ H_{y,p}(x,y) \end{pmatrix} = \sum_{m,n,p} e^{ik_0(\alpha m x + \beta_n y)} V_{mn,p} \tag{4}$$

and its x-y distribution (and $V_{mn,p}$, in particular) does not depend on the z-direction, because the grating shape is invariant in z.

An important technical remark is due: in presence of mode degeneration (two or more modes having the same value of γ), it is necessary to consider an appropriate linear combination of these modes, with coefficients determined by the corresponding modal amplitudes b_p. This is always the case of two-dimensional high-symmetry gratings that modes appear in couples with two mutually orthogonal polarizations.

#264075 Received 26 Apr 2016; revised 14 Jun 2016; accepted 14 Jun 2016; published 23 Jun 2016

Figure 4(a) presents the normalized propagation constants $n_{eff} = \gamma_p / k_0$ for the modes that propagate in the structure along the z-direction (i.e., having lossless propagation constant $\mathrm{Im}(\gamma_p) = 0$). In fact, there is either only a single mode, or three modes, each of which is twice degenerated. Each of them can propagate upwards or downwards so that for each γ_p it exists a mode with $-\gamma_p$. Their amplitudes will be noted as b_p^+ and b_p^-, respectively. In what follows, we shall call these modes 'vertical modes'.

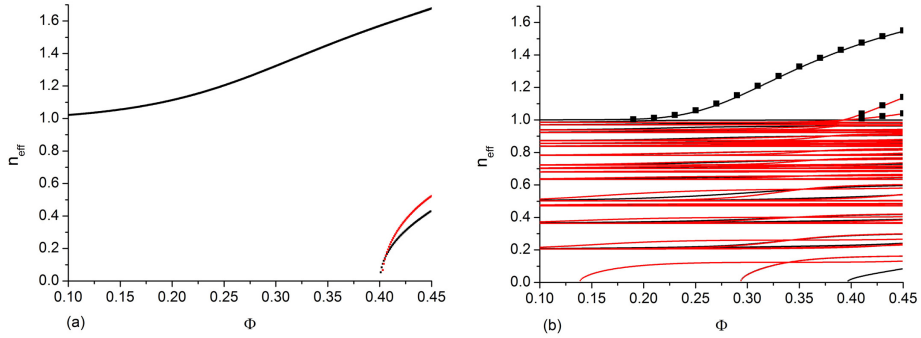

Fig. 4. (a). The dependence of the mode effective index $n_{eff} = \gamma_p/k_0$ equal to the normalized propagation constant γ in z-direction as a function of the cylinder diameter. d = 0.5 μm, λ = 0.865 μm. The red line corresponds to a mode that cannot be excited with linear incident polarization in normal incidence; (b) the same as in (a) but for d = 5 μm. In addition, the squares stay for the modes that can propagate along a single infinitely long fiber.

For narrower cylinders, only a single mode has a real propagating constant and it is larger than 1. If instead of a set of fibers, we consider a single one, this case represents the fundamental mode of a single step-index fiber with evanescent field in the surrounding air. If we consider a long-period grating (5 μm instead of 0.5 μm), where the fibers are separated by large distances and the propagating modes do not interact mutually (via evanescent field of the mode), the modes have exactly the same propagation constants, as those calculated for a single step-index fiber, as can be observed in Fig. 4(b). The calculations for a single step-index fiber are made by solving the transcendental equation obtained by applying continuities of the fields (written as Fourier-Bessel expansions) at the fiber circular interface [23, 24].

As the fiber diameter increases, the vertical mode propagation constant increases gradually, both in the case of a single fiber, long- and short-period grating, and with the larger diameter, new guided modes appear. The first new ones, represented with dots on the red curve in Fig. 4(b) correspond to the TE_{01} and TM_{01} modes of the single fiber [25]. They have azimuthal or radial polarization, with electric field antisymmetrical with respect the fiber axis, thus they cannot be excited with a linearly polarized light, because the overlap integrals (scalar products) between their electric fields and the incident field vanish. Moreover, for short-period gratings, the coupling between the guided modes in the closely lying cylinders increases, as is discussed further on.

In addition to these vertical modes, there exists in Fig. 4(b) a large family of other modes ($\mathrm{Re}(n_{eff}) < 1$) that does not exist in a single fiber – these are almost plane waves that can propagate in the x-y plane, as discussed in detail later. They represent collective modes of the grating structure; in what follows they are called 'horizontal modes'. For the short-period grating, this family (which becomes quite different from the plane wave approximation) of modes reduces to only two, one of which cannot be excited with linearly polarized incident light.

We present in Table 1 the values of the normalized propagation constant for the three modes when λ = 0.865 μm and Φ = 0.4333 μm. The imaginary part of the propagation constant is within the machine error, so that we consider that these modes have real

#264075 Received 26 Apr 2016; revised 14 Jun 2016; accepted 14 Jun 2016; published 23 Jun 2016

propagation constant. The first two are twice degenerated; the second pair is noted as mode 1' and mode 2' and they participate in the diffraction process if the incident wave is polarized along y-direction. As far as we use incident wave polarized along x, the amplitudes of these secondary modes are negligible when compared to modes 1 and 2. The slight difference in the values of n_{eff} in each pair is probably due to the asymmetry in the prolongation of the vector normal to the cylinder surface because we perform an analytical 2D Fourier decomposition of the permittivity, instead of FFT [26]. One can observe, in addition, that mode 3 is not excited (the electric field values are of the order of the computer error) in normal incidence because of its symmetry. Its electric field (the modulus given in Fig. 5) has azimuthal direction in each cylinder and thus is antisymmetrical in Cartesian coordinates, as already discussed with respect to Fig. 4(b). All over the paper, the incident electric field amplitude is taken to be equal to one, and the field maps are normalized with respect to the incident wave modulus.

Table 1. The values of the real part of the normalized mode propagation constant for the different modes of a system with d = 0.5 μm, Φ = 0.4333 μm, λ = 0.865 μm, together with the modulus of the up- and downwards traveling mode amplitudes b for h = 1 μm.

	$Re(n_{eff})$	b +	b–
mode 1	1,64182	0,67963328	0,6819777
mode 2	0,3556	2,13137972	2,13108853
mode 3	0,43448	1,04E-12	1,34E-12
mode 1'	1,64103	0,00004620	0,00003548
mode 2'	0,35547	0,00011827	0,00010419

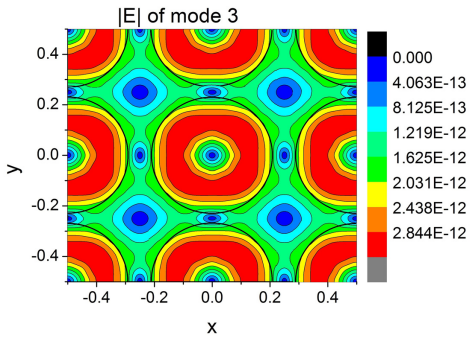

Fig. 5. The map of the modulus of the electric field of mode 3 as a function of x and y, Φ = 0.4333 μm and λ = 0.865 μm, and normal incidence. All coordinates are given in microns.

There exist a direct link between the modes of distant fibers and of the subwavelength grating. Figure 6 presents the dependence of n_{eff} on the groove period for a fixed cylinder dimensions, corresponding to that giving the reflection maximum in Fig. 3(a). We observe a gradual transfer from one set of modes to another. Decreasing the distance between the fibers, the vertical modes ($n_{eff} > 1$) couple between each other, and n_{eff} increases because the average refractive index decreases with the filling factor $f = \pi\Phi^2 / d^2$, Fig. 6(a). The red dashed curve presents the valus of the normalizedpropagation constant of the next mode (4) that is below its cut-off for d < 0.75 μm, and that plays no role in the diffraction process for d = 0.5 μm.

#264075 Received 26 Apr 2016; revised 14 Jun 2016; accepted 14 Jun 2016; published 23 Jun 2016

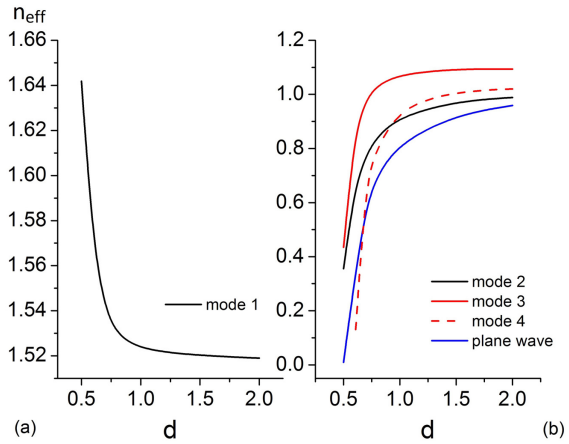

Fig. 6. Variation of n_{eff} as a function of the period d for a fixed cylinder diameter Φ = 0.4333 μm and λ = 0.865 μm, and normal incidence.

On the contrary, for the collective, horizontal modes, the values of n_{eff} decrease when d decreases. This behavior can be understood by using a quite approximate plane-wave model and average refractive index values, represented by the blue curve in Fig. 6(b). If the plane wave that can propagate in the x-y plane is excited in normal incidence through the first diffracted orders of the grating, having normalized wavevector amplitude in x or y direction simply equal to λ/d, so that in z-direction we obtain:

$$n_{eff} = \sqrt{\bar{\varepsilon}_r - (\lambda / d)^2}, \tag{5}$$

where $\bar{\varepsilon}_r = = f\, n_f^2 + (1-f)$ is the average relative permittivity of the grating region, $n_f = 1.97$. As can be observed in Fig. 6(b), the behavior of the collective horizontal modes is quite well expressed qualitatively by Eq. (5).

4. Electric field distributions

Deeper physics knowledge can be obtained from the field maps, rather than the modal analysis of the propagation constants. In particular, we show in this section that the transition from large- to short-period gratings leads to a stronger localization of the modes in the structure, which explains the large angular tolerances observed in Fig. 3(b). We return to the original problem discussed in Sec.2: an array of truncated rods on a glass substrate illuminated by a plane wave.

The accuracy of the Fourier modal method numerical results described in Sec. 2 and 4 has been checked by comparing it to the results of the finite element formulation described in [27, 28]. This FEM formulation allows computing numerically the vector fields diffracted by any arbitrarily shaped crossed grating embedded in a multilayered stack in the time-harmonic regime. The field maps obtained by the FEM show a quite good agreement with the results of the Fourier modal method, which confirms the validity of the results.

The field maps confirm the conclusion already made and, in addition, show a gradual localization of the field intensities in space when the grating period diminishes, which explains finally the large angular tolerance of the reflectivity maximum observed in Fig. 3(b).

Let us consider the evolution of the modal field maps (modulus of the electric field) for the two modes (mode 1 and mode 2 as noted in Table 1) for two different grating periods, d = 2 and 0.5 μm in Fig. 7. For a large distance between the cylinders, as expected, mode 1 is localized mainly inside the fiber, while mode 2 has a minimum of the field in the fiber and has an almost constant intensity in the surrounding space, as for a plane wave in the x-y plane. These modes are localized in much smaller regions for the subwavelength grating (d = 0.5 μm). Mode 1 becomes strongly localized in-between the close points of the cylinders (Fig.

#264075 Received 26 Apr 2016; revised 14 Jun 2016; accepted 14 Jun 2016; published 23 Jun 2016

7(e)), while mode 2 field distribution resembles a dipole along the x-axis (incident wave is polarized along the x-axis). The total field of the grating structure with h = 1 μm represents a superposition of the two modes

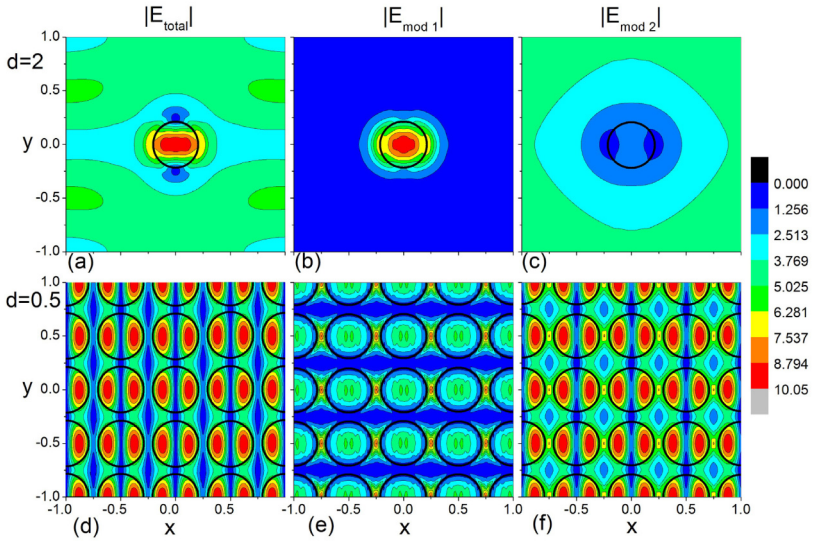

Fig. 7. x-y maps of the modulus of electric field of mode 1 (b, e), mode 2 (c, f), and the total field (a,d) for two grating periods, d = 2 μm (a-c) and 0.5 μm (d-f) for a fixed cylinder diameter 0.4333 μm, wavelength 0.865 μm and polarization along x-direction. The modal fields calculated for a 2D array of rods infinitely long in z does not depend on z-direction, while the total field, which is a solution of the 3D diffraction problem is calculated at mid-height z = 0.5 μm with h = 1 μm. Black circles represent the cylinder boundaries.

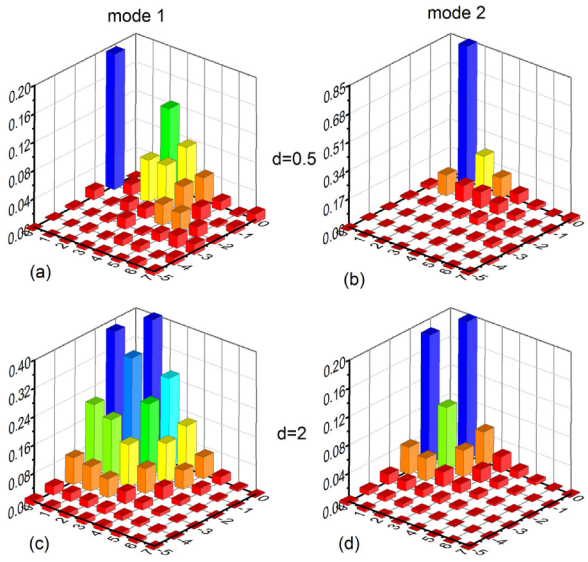

Fig. 8. Fourier spectrum of the x-components of the electric field of mode 1 and mode 2, corresponding to Fig. 7 for two different period values. Vertical axis represent the values of the modulus of the Fourier components, numbered on the horizontal axis.

Fourier analysis in Fig. 8 of the predominant field component (E_x) of each mode confirms the presumptions that mode 1 is much more localized in the direct space (larger Fourier spectrum) than mode 2. The larger Fourier spectrum and the enhanced spatial localization

#264075 Received 26 Apr 2016; revised 14 Jun 2016; accepted 14 Jun 2016; published 23 Jun 2016

express in larger angular tolerances. In addition, mode 2 is characterized by a predominant first Fourier harmonic, which represents a wave propagating in x-direction that has almost plane-wave distribution for d = 2 μm, and is much more structured for d = 0.5 μm, because it is formed as a standing wave due to the interference of order + 1 and –1 in x or y.

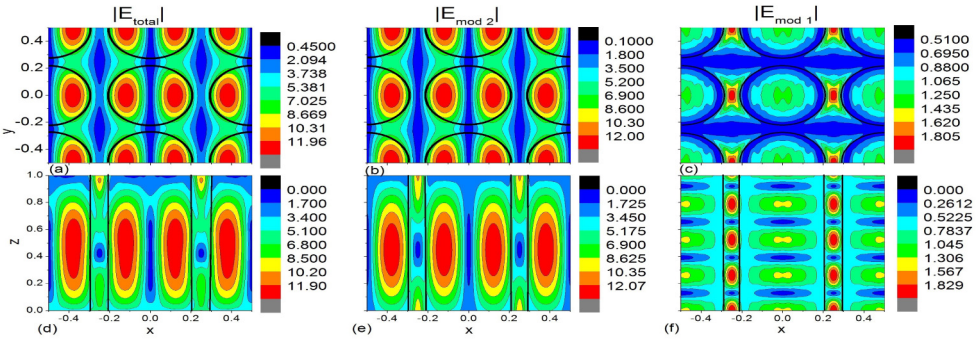

Fig. 9. Vertical (d-f) and horizontal (a-c) distribution of electric field, calculated by taking into account all existing modes (a, d), mode 1 only (c, f), or mode 2 alone (b, e). The vertical maps are calculated at y = 0, and the horizontal maps at z = 0.5. The cylinder boundaries are presented by black circles or lines.

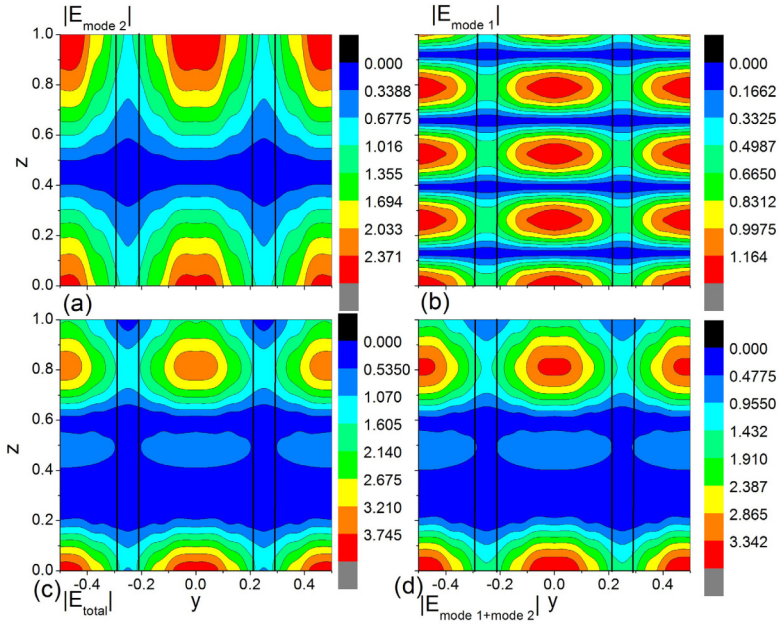

Fig. 10. The y-z field maps calculated at x = 0 and taking into account different modal contributions: (a) mode 2 alone; (b) mode 1 alone; (d) mode 1 and mode 2; (c) all modal components

Additional study for the intermediate values of d not reported here shows a gradual transfer from the field maps from d = 2 to d = 0.5 μm.

After having analyzed the mode fields of the two different modes that have real propagating z-constants in z, a natural question arises – what is the role of each of them for obtaining a 100% reflection maximum in Fig. 3(a).

#264075 Received 26 Apr 2016; revised 14 Jun 2016; accepted 14 Jun 2016; published 23 Jun 2016

Let us at first compare the field maps of the total field $|E_{tot}(x,y)|$ calculated using all the modes with the field distribution of the separate modes $|E_{mode\,1}(x,y)|$ and $|E_{mode\,2}(x,y)|$ by taking into account the true values of the mode amplitudes b_p and the fact that there are up- and down-going modes in the structure. This means that for each mode we take the four components coming from the double degenerating and for the two signs of γ. These field maps are presented in Figs. 9 and 10, for the xy, xz, and yz cuts. There are several conclusions that can be made:

(1) xz-cut clearly shows that mode 2 is much stronger than mode 1 and that it approaches quite well the total field distribution (Fig. 9(d)-9(f));

(2) the same conclusion is valid for the xy map in the middle of the height (z = 0.5 μm) (Fig. 9(a)-9(c));

(3) on the contrary, the slices for which mode 2 is weaker (yz for x = 0, or xy for z = 0 and h, the last two not shown here), mode 1 is as important as mode 2 in the total field maps. In particular, Fig. 10 shows that the yz slice for x = 0 of the total field requires the participation of both mode 1 and mode 2 in the total field reconstruction.

These conclusions confirm the analysis in the one-dimensional case made by Lalanne [13] that it is required to have the excitation of two simultaneous modes in order to obtain high reflectivity with a plateau in the angular dependency. Moreover, we are able to further extend the numerical experiment by forcing the rigorous Fourier Modal Method to calculate the reflectivity by working with only a single or several z-modes, instead of all modes that are necessary for the rigorous solution of the Maxwell equations and the boundary conditions at z = 0 and h (and the outgoing wave conditions above and below the grating). To this aim, the calculations of the eigenvalues and the eigenvectors of the M-matrix in Eq. (1) are correctly done. Then, the imaginary parts of all the eigenvalues, except some specific ones is increased drastically to ensure that they are completely damped between z = 0 and z = h, so their participation in the energy transfer between the upper to the lower interface becomes negligible. However, all the modes are taken into account in satisfying the boundary conditions at z = 0 and z = h.

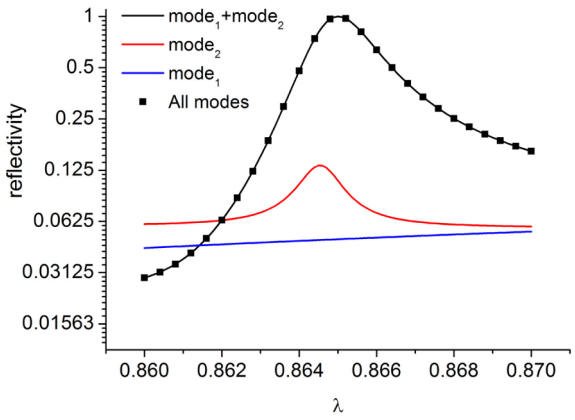

Fig. 11. Spectral dependence of the reflectivity corresponding to Fig. 3(a) and obtained by suppressing all other modes than mode 1 (blue), or mode 2 (red), or both of them (black). The squares are obtained by using the complete modal set.

Figure 11 presents the reflectivity by taking into account the total number of modes (points), only mode 1 and modes 2, separately only mode 1 or mode 2. Quite amazingly, mode 1 and mode 2 are perfectly sufficient to reproduce the Fano-type resonance (asymmetrical Lorentzian containing both a pole and a zero), while mode 1 reproduces a

#264075 Received 26 Apr 2016; revised 14 Jun 2016; accepted 14 Jun 2016; published 23 Jun 2016

Fabry-Perot weak resonance (without a peak appearing inside the spectral interval given in the figure). The single mode 2 leads to a Lorenzian-shape resonance at the same spectral position as the true curve, but it does not reach 100%. The energy balance is neitherfulfilled in the last two cases.

The reason seems obvious: When a single mode is taken into account, either a Fabry-Perot resonance in z-direction, having weak reflection coefficients at z = 0 and z = h appears for a single mode 1, or stronger Lorentz-type resonance is participating with mode 2 that "propagates" in the xy-plane (similar to a waveguide mode for classical gratings). However, despite the resonance behavior in both case of single-mode contribution, they cannot lead to a 100% maximum in the reflectivity due to the following reason. This value of the maximum is due to the fact that in the Fano-type anomaly, the zero in transmission is real for such symmetry of the structure. However, the existence of a zero in transmission (or, more general, also in reflection) for a Fano anomaly requires as a minimum two independent contribution, a resonant and a non-resonant one (or, why not, two resonant ones, although it goes outside the Fano contribution) in order to create a zero from the Lorentzian anomaly:

$$t_{Fano} = t_{nonresonant} + t_{Lorentz} = t_{nonresonant} + \frac{c}{\lambda - \lambda^p} = t_{nonresonant} \frac{\lambda - \lambda^z}{\lambda - \lambda^p} \tag{6}$$

with $\lambda^z = \lambda^p - \frac{c}{t_{nonresonant}}$, where t stays for the transmission, c is a slowly varying function, corresponding to a coupling coefficient between the incident field and the mode, the subscript p stays for the pole and z for the zero. Without the nonresonant contribution, the zero of the Lorenzian curve is sent to $\lambda \to \infty$.

Same is valid for two resonant contributions:

$$\begin{aligned} t_{Fano} &= \frac{c_1}{\lambda - \lambda_1^p} + \frac{c_2}{\lambda - \lambda_2^p} = (c_1 + c_2) \frac{\lambda - \lambda^z}{\left(\lambda - \lambda_1^p\right)\left(\lambda - \lambda_2^p\right)} \\ \lambda^z &= \frac{c_1 \lambda_2^p + c_2 \lambda_1^p}{c_1 + c_2}, \end{aligned} \tag{7}$$

which represents Fano anomaly if only both $c_{1,2} \neq 0$, otherwise it rests Lorentzian.

Acknowledgment

The support of the ANR funded project PLANISSIMO (ANR-12-NANO-0003) is gratefully acknowledged.